NJC

Accepted Manuscript

This article can be cited before page numbers have been issued, to do this please use: F. Asghar, S. Rana, S. Fatima, A. Badshah, B. Lal and I. S. Butler, *New J. Chem.*, 2018, DOI: 10.1039/C8NJ00483H.

ROYAL SOCIETY OF CHEMISTRY

rsc.li/njc

View Article Online
DOI: 10.1039/C8NJ00483H

Biologically active *halo*-substituted ferrocenyl thioureas: Synthesis, spectroscopic characterization, and DFT calculations

Faiza Asghar[a*, b, c], Sadaf Rana[b], Saira Fatima[b], Amin Badshah[b*], Bhajan Lal[d], Ian S. Butler[c]

*. Corresponding Authors:
Department of Chemistry, University of Wah, Quaid Avenue, Wah (47000), Pakistan.
faiza994@hotmail.com
Department of Chemistry, Quaid-i-Azam University, Islamabad (45320), Pakistan.
aminbadshah@yahoo.com

a. Department of Chemistry, University of Wah, Quaid Avenue, Wah (47000), Pakistan.
b. Department of Chemistry, Quaid-i-Azam University, Islamabad (45320), Pakistan.
c. Department of Chemistry, McGill University, Montreal, QC, Canada H3A 2K6.
d. Institute of Chemistry, Shah Abdul Latif University, Khairpur-66020, Pakistan.

Abstract

In our search for new therapeutic agents, ferrocene-based thioureas **(M1-M9)** were successively synthesized and characterized by various analytical techniques like: FT-IR, Raman, CHNS, AAS, and multinuclear (^{1}H and ^{13}C) NMR. The interaction of the compounds with DNA was investigated by electrochemical and spectroscopic measurements. These complexes exhibited impressive binding constants ranging from 9.75 x 10^{3} to 5.71 x 10^{4} M^{-1}. The diffusion coefficients of the drug-DNA adducts are lower than is that for the free drug indicating the formation of a high molecular weight complex that diffuses slowly towards the electrode. The cathodic peak potential shift in the cyclic voltammetric behavior of the synthesized complexes by the addition of DNA is attributable to the electrostatic interactions between the compound and DNA, an indicator of the oxidizable behavior of the compounds in the presence of negative environment of DNA. The energy of frontier molecular orbitals (E_{HOMO} and E_{LUMO}) and the Mulliken charge distribution on the optimized structures was determined using DFT/B3LYP method combined with 6-31G(d,p) basis set in DMSO. The theoretically calculated HOMO and LUMO energies (HOMO-LUMO band gap) based on DFT study correlate well with the electrochemically determined redox potentials (electrochemical band gap), having a correlation coefficient of 0.953. The synthesized thioureas were preliminary screened for their *in vitro* antimicrobial, and cytotoxic activities. However, the most significant antitumor activity was found for **M3** with IC_{50} value of 1.87 µM. These compounds played a significant role in arresting microbial growth. The computational measurements were found to be in close agreement with the outcomes of biological activities.

View Article Online
DOI: 10.1039/C8NJ00483H

Keywords: Ferrocene; DNA binding; DFT study; Anticancer activity; Antimicrobial.

1. Introduction

Interest in metal complexes with therapeutic applications has developed at a tremendous rate since the discovery of cisplatin as an effective antitumor agent.[1,2] Nowadays, the most promising non-platinum cytotoxic drugs are evolving from the arena of bio-organometallics.[3,4] Metallocenes contain an entire class of numerous transition metals such as: V(II), Cr(II), Co(II), Ru(II) and Ni(II), nevertheless ferrocene still serves the foremost motivation of research chiefly due to its notable stability and ease of preparation.[5] Ferrocene is also a particularly attractive candidate for integration into biomolecules due to its aromaticity, redox properties, and low toxicity. Ferrocifen, the ferrocene analogue of hydroxytamoxifen shows enhanced inhibitory effect against hormone-dependent and independent breast cancer cells.[6,7] The anticancer activities of ferrocenyl derivatives generally depend upon the oxidation state of iron (Fe), with Fe^{2+} derivatives more active than Fe^{3+} derivatives, by changing the conformation of receptor protein.[8,9] According to Osella et al.,[10] anticancer activity arises due to generation of oxygen active radicals by the reduction of ferrocenium ion. The cytotoxicity of compounds is due to the interaction with DNA by which the physical and chemical nature of DNA alters.[11]

Thioureas display comprehensive range of bio-activities comprising: antiviral,[12,13] antibacterial,[14] antifungal,[15] antitubercular,[16] herbicidal,[17] insecticidal,[18] and pharmaco-dynamic properties,[19] act as corrosion inhibitors, free radical scavengers, and are polymer constituents.[20,21] Acyl thiourea derivatives are well-recognized for their pharmacological potential such as: anti-inflammatory, bactericidal, fungicidal, and plant growth regulatory activity.[22,23] One of the chief concerns associated with thiourea derivatives is a high dose is required for the treatment due to their low lipophilicity, which restrains their efficiency and imparts lot of lethal side effects.[24] This problem can be overwhelmed by introducing a lipophilic moiety such as ferrocene in the thiourea structure, which will minimize the side effects due to its enhanced lipid soluble potential.[25]

The primary characteristic of the contemporary pharmaceutical investigation and development demands presenting novel candidates for several biological targets. To further explore the prominence of ferrocene-incorporated thioureas in medicinal chemistry, herein we report the synthesis, structural characterization, and *in vitro* biological studies of some

View Article Online
DOI: 10.1039/C8NJ00483H

new N,N′-disubstituted ferrocenyl thioureas for their DNA binding efficiency, antimicrobial, and anticancer properties. Moreover, the DFT study was also accomplished on these structures to theoretically determine the energy of frontier molecular orbitals, vibrational frequencies, and the Mulliken charge distribution on the molecular structures.

2. Experimental

2.1 Materials and methods

Melting points were determined in a capillary tube using an electro-thermal melting point apparatus model MP-D Mitamura Riken Kogyo (Japan). Infrared spectra were taken on a Thermoscientific NICOLET 6700 FT-IR instrument. ^{1}H- and ^{13}C-NMR data were recorded on a Bruker AV500 MHz spectrometer in DMSO. $Si(CH_3)_4$ was used as an internal reference. Raman spectra (± 1 cm^{-1}) were measured on an InVia Renishaw spectrometer, using argon-ion (514.5 nm) and near-infrared diode (785 nm) lasers. The Renishaw WiRE 2.0 software was used for the Raman data acquisition and spectral manipulation. The elemental analyses were performed using a LECO-932 CHNS analyzer, while the Fe concentrations were determined on an atomic absorption spectrophotometer Perkin Elmer 2380.

Ferrocene, 2-methoxy-5-nitroaniline, sodium nitrite, diethyl ether, acetone, Zn dust, DMSO, ammonium formate, KSCN, and acid chlorides such as: *o*-fluorobenzoyl chloride, *m*-fluorobenzoyl chloride, *p*-fluorobenzoyl chloride, *o*-chlorobenzoyl chloride, *m*-chloro benzoyl chloride, *p*-chlorobenzoyl chloride, *o*-bromobenzoyl chloride, *m*-bromobenzoyl chloride, and *p*-bromo benzoyl chloride were obtained from commercial sources (Sigma Aldrich/Fluka) and used as received. 4-methoxy-3-ferrocenylaniline was synthesized by a procedure reported by our group previously (Step 1, Scheme 1).[26,27]

2.2 General procedure for the synthesis of ferrocene-based acyl thioureas **(M1-M9)**

The synthesis of ferrocene incorporated thioureas was accomplished by adopting the method reported previously by our group with some modifications.[28] To the suspension of potassium thiocyanate (10 mmol) in dry acetone (50-60 mL), different acid chlorides (10 mmol) were introduced under an inert atmosphere (N_2) leading to the preparation of the respective isothiocyanates. 4-methoxy-3-ferrocenylaniline (10 mmol) was then added to the resulting reaction mixtures, which were then stirred for 12 h. Afterwards, the reaction mixtures were transferred to ice cold water and stirred well in order to remove water soluble

View Article Online
DOI: 10.1039/C8NJ00483H

impurities. The solid products were separated by filtration and washed with deionized water. The residues were then dissolved in dichloromethane/chloroform and kept for crystallization (Scheme 1).

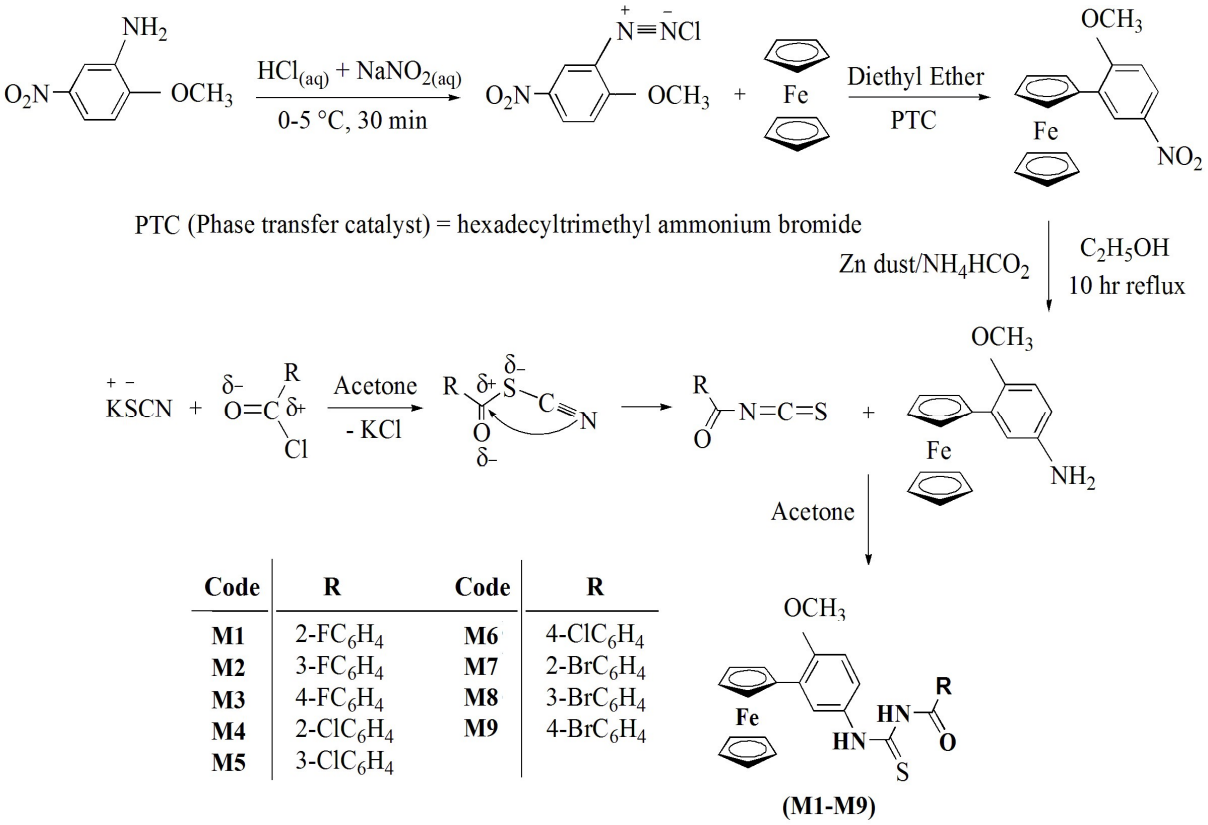

Scheme 1. Synthetic scheme for ferrocene-based thioureas.

2.2.1 1-(2-fluorobenzoyl)-3-(4-methoxy-3-ferrocenylphenyl)thiourea **(M1)**

Quantities used were 2.92 g (10 mmol) 4-methoxy-3-ferrocenylaniline, 0.98 g (10 mmol) potassium thiocyanate, and 1.20 ml (10 mmol) of 2-fluorobenzoyl chloride. Yield 77%; Brown solid; m.p. 204 °C; FT-IR and Raman (powder, cm^{-1}): 3392-3227 (N-H), 3079, 3025 (C-$H_{aromatic}$), 2946, 2910 (C-$H_{aliphatic}$), 1663, 1671 (C=O), 1602, 1593 (C=C), 1257-1138 cm^{-1} (C=S), 481, 483 (Fe-Cp); ^{1}H-NMR (500 MHz, DMSO-d_6, ppm) δ 12.26 (s, 1H, NH), 11.52 (s, 1H, NH), 7.98-7.35 (m, 7H, ArH), 4.65 (s, 2H, C_5H_4), 4.36 (s, 2H, C_5H_4), 4.16 (s, 5H, C_5H_5), 3.55 (s, 3H, OCH_3); ^{13}C-NMR (125.81 MHz, DMSO-d_6, ppm) δ 177.5, 169.7, 162.6, 140.8, 138.9, 136.4, 134.5, 132.1, 127.6, 124.9, 122.7, 118.8, 116.6, 86.7, 70.2, 69.3, 67.9, 57.4; Elemental anal. Calcd. (%) for $C_{25}H_{21}FFeN_2O_2S$: C, 61.52; H, 4.35; N, 5.78; S, 6.56; Fe, 11.41. Found (%): C, 61.41; H, 4.26; N, 5.69; S, 6.64; Fe, 11.32.

View Article Online
DOI: 10.1039/C8NJ00483H

2.2.2 1-(3-fluorobenzoyl)-3-(4-methoxy-3-ferrocenylphenyl)thiourea **(M2)**

Quantities used were 2.92 g (10 mmol) 4-methoxy-3-ferrocenylaniline, 0.98 g (10 mmol) potassium thiocyanate, and 1.22 ml (10 mmol) of 3-fluorobenzoyl chloride. Yield 70%; Brown solid; m.p. 197 °C; FT-IR and Raman (powder, cm^{-1}): 3360-3217 (N-H), 3074, 3059 (C-$H_{aromatic}$), 2935, 2952 (C-$H_{aliphatic}$), 1665, 1674 (C=O), 1590, 1598 (C=C), 1261-1143 cm^{-1} (C=S), 478, 482 (Fe-Cp); ^{1}H-NMR (500 MHz, DMSO-d_6, ppm) δ 12.33 (s, 1H, NH), 11.60 (s, 1H, NH), 7.92-7.31 (m, 7H, ArH), 4.73 (s, 2H, C_5H_4), 4.40 (s, 2H, C_5H_4), 4.09 (s, 5H, C_5H_5), 3.74 (s, 3H, OCH_3); ^{13}C-NMR (125.81 MHz, DMSO-d_6, ppm) δ 178.4, 167.5, 162.8, 141.1, 138.7, 136.5, 134.7, 132.4, 128.2, 123.4, 121.3, 117.5, 115.8, 87.0, 70.7, 69.5, 67.2, 56.5; Elemental anal. Calcd. (%) for $C_{25}H_{21}FFeN_2O_2S$: C, 61.52; H, 4.35; N, 5.78; S, 6.56; Fe, 11.41. Found (%): C, 61.60; H, 4.33; N, 5.72; S, 6.47; Fe, 11.49.

2.2.3 1-(4-fluorobenzoyl)-3-(4-methoxy-3-ferrocenylphenyl)thiourea **(M3)**

Quantities used were 2.92 g (10 mmol) 4-methoxy-3-ferrocenylaniline, 0.98 g (10 mmol) potassium thiocyanate, and 1.18 ml (10 mmol) of 4-fluorobenzoyl chloride. Yield 67%; Brown solid; m.p. 188 °C; FT-IR and Raman (powder, cm^{-1}): 3374-3233 (N-H), 3086, 3061 (C-$H_{aromatic}$), 2931, 2941 (C-$H_{aliphatic}$), 1676, 1665 (C=O), 1591, 1588 (C=C), 1268-1147 cm^{-1} (C=S), 483, 473 (Fe-Cp); ^{1}H-NMR (500 MHz, DMSO-d_6, ppm) δ 12.75 (s, 1H, NH), 11.67 (s, 1H, NH), 8.01-7.46 (m, 7H, ArH), 4.66 (s, 2H, C_5H_4), 4.35 (s, 2H, C_5H_4), 4.06 (s, 5H, C_5H_5), 3.68 (s, 3H, OCH_3); ^{13}C-NMR (125.81 MHz, DMSO-d_6, ppm) δ 179.1, 165.4, 161.6, 140.5, 138.7, 135.9, 133.4, 132.2, 129.5, 125.4, 122.3, 117.9, 115.7, 86.6, 70.2, 69.7, 66.5, 55.1; Elemental anal. Calcd. (%) for $C_{25}H_{21}FFeN_2O_2S$: C, 61.52; H, 4.35; N, 5.78; S, 6.56; Fe, 11.41. Found (%): C, 61.44; H, 4.23; N, 5.71; S, 6.66; Fe, 11.35.

2.2.4 1-(2-chlorobenzoyl)-3-(4-methoxy-3-ferrocenylphenyl)thiourea **(M4)**

Quantities used were 2.92 g (10 mmol) 4-methoxy-3-ferrocenylaniline, 0.98 g (10 mmol) potassium thiocyanate, and 1.26 ml (10 mmol) of 2-chlorobenzoyl chloride. Yield 74%; Brown solid; m.p. 213 °C; FT-IR and Raman (powder, cm^{-1}): 3388-3212 (N-H), 3076, 3091 (C-$H_{aromatic}$), 2927, 2936 (C-$H_{aliphatic}$), 1668, 1661 (C=O), 1593, 1596 (C=C), 1265-1132 cm^{-1} (C=S), 475, 486 (Fe-Cp); ^{1}H-NMR (500 MHz, DMSO-d_6, ppm) δ 12.33 (s, 1H, NH), 11.61 (s, 1H, NH), 7.88-7.36 (m, 7H, ArH), 4.68 (s, 2H, C_5H_4), 4.41 (s, 2H, C_5H_4), 4.13 (s, 5H, C_5H_5), 3.77 (s, 3H, OCH_3); ^{13}C-NMR (125.81 MHz, DMSO-d_6, ppm) δ 178.2, 168.3, 139.3, 137.6, 134.7, 133.9, 131.6, 129.3, 125.1, 121.8, 117.2, 115.6, 86.2, 69.8, 68.4, 66.2,

View Article Online
DOI: 10.1039/C8NJ00483H

56.3; Elemental anal. Calcd. (%) for $C_{25}H_{21}ClFeN_2O_2S$: C, 59.46; H, 4.16; N, 5.53; S, 6.31; Fe, 11.08. Found (%): C, 59.36; H, 4.08; N, 5.62; S, 6.23; Fe, 11.01.

2.2.5 1-(3-chlorobenzoyl)-3-(4-methoxy-3-ferrocenylphenyl)thiourea **(M5)**

Quantities used were 2.92 g (10 mmol) 4-methoxy-3-ferrocenylaniline, 0.98 g (10 mmol) potassium thiocyanate, and 1.28 ml (10 mmol) of 3-chlorobenzoyl chloride. Yield 66%; Brown solid; m.p. 195 °C; FT-IR and Raman (powder, cm^{-1}): 3364-3204 (N-H), 3088, 3054 (C-$H_{aromatic}$), 2951, 2944 (C-$H_{aliphatic}$), 1672, 1664 (C=O), 1595, 1591 (C=C), 1260-1136 cm^{-1} (C=S), 485, 478 (Fe-Cp); ^{1}H-NMR (500 MHz, DMSO-d_6, ppm) δ 12.42 (s, 1H, NH), 11.57 (s, 1H, NH), 7.81-7.50 (m, 7H, ArH), 4.72 (s, 2H, C_5H_4), 4.33 (s, 2H, C_5H_4), 4.11 (s, 5H, C_5H_5), 3.59 (s, 3H, OCH_3); ^{13}C-NMR (125.81 MHz, DMSO-d_6, ppm) δ 177.1, 167.0 140.6, 138.7, 135.8, 132.3, 130.9, 129.1, 125.8, 122.4, 116.6, 114.3, 86.5, 70.3, 69.7, 66.8, 54.8; Elemental anal. Calcd. (%) for $C_{25}H_{21}ClFeN_2O_2S$: C, 59.46; H, 4.16; N, 5.53; S, 6.31; Fe, 11.08. Found (%): C, 59.54; H, 4.25; N, 5.44; S, 6.39; Fe, 11.17.

2.2.6 1-(4-chlorobenzoyl)-3-(4-methoxy-3-ferrocenylphenyl)thiourea **(M6)**

Quantities used were 2.92 g (10 mmol) 4-methoxy-3-ferrocenylaniline, 0.98 g (10 mmol) potassium thiocyanate, and 1.30 ml (10 mmol) of 4-chlorobenzoyl chloride. Yield 75%; Brown solid; m.p. 192 °C; FT-IR and Raman (powder, cm^{-1}): 3391-3223 (N-H), 3055, 3083 (C-$H_{aromatic}$), 2949, 2934 (C-$H_{aliphatic}$), 1669, 1672 (C=O), 1587, 1596 (C=C), 1253-1154 cm^{-1} (C=S), 481, 474 (Fe-Cp); ^{1}H-NMR (500 MHz, DMSO-d_6, ppm) δ 12.52 (s, 1H, NH), 11.73 (s, 1H, NH), 7.77-7.48 (m, 7H, ArH), 4.77 (s, 2H, C_5H_4), 4.45 (s, 2H, C_5H_4), 4.16 (s, 5H, C_5H_5), 3.83 (s, 3H, OCH_3); ^{13}C-NMR (125.81 MHz, DMSO-d_6, ppm) δ 179.9, 168.7, 141.5, 139.3, 136.9, 134.4, 133.0, 131.7, 126.8, 123.5, 118.2, 116.1, 87.2, 70.7, 69.6, 66.8, 58.5; Elemental anal. Calcd. (%) for $C_{25}H_{21}ClFeN_2O_2S$: C, 59.46; H, 4.16; N, 5.53; S, 6.31; Fe, 11.08. Found (%): C, 59.37; H, 4.05; N, 5.59; S, 6.25; Fe, 11.05.

2.2.7 1-(2-bromobenzoyl)-3-(4-methoxy-3-ferrocenylphenyl)thiourea **(M7)**

Quantities used were 2.92 g (10 mmol) 4-methoxy-3-ferrocenylaniline, 0.98 g (10 mmol) potassium thiocyanate, and 1.30 ml (10 mmol) of 2-bromobenzoyl chloride. Yield 63%; Brown solid; m.p. 206 °C; FT-IR and Raman (powder, cm^{-1}): 3382-3219 (N-H), 3064, 3081 (C-$H_{aromatic}$), 2944, 2926 (C-$H_{aliphatic}$), 1674, 1663 (C=O), 1594, 1589 (C=C), 1266-1125 cm^{-1} (C=S), 488, 479 (Fe-Cp); ^{1}H-NMR (500 MHz, DMSO-d_6, ppm) δ 12.29 (s, 1H, NH), 11.06 (s, 1H, NH), 7.93-7.45 (m, 7H, ArH), 4.66 (s, 2H, C_5H_4), 4.40 (s, 2H, C_5H_4), 4.13 (s,

View Article Online
DOI: 10.1039/C8NJ00483H

5H, C_5H_5), 3.74 (s, 3H, OCH_3); ^{13}C-NMR (125.81 MHz, DMSO-d_6, ppm) δ 178.7, 168.2, 138.7, 136.5, 134.8, 133.6, 132.5, 131.6, 129.4, 127.7, 122.2, 118.3, 87.5, 70.6, 69.4, 68.5, 56.8; Elemental anal. Calcd. (%) for $C_{25}H_{21}BrFeN_2O_2S$: C, 54.64; H, 3.91; N, 5.13; S, 5.89; Fe, 10.19. Found (%): C, 54.73; H, 3.98; N, 5.02; S, 5.80; Fe, 10.27.

2.2.8 1-(3-bromobenzoyl)-3-(4-methoxy-3-ferrocenylphenyl)thiourea **(M8)**

Quantities used were 2.92 g (10 mmol) 4-methoxy-3-ferrocenylaniline, 0.98 g (10 mmol) potassium thiocyanate, and 1.32 ml (10 mmol) of 3-bromobenzoyl chloride. Yield 67%; Brown solid; m.p. 192 °C; FT-IR and Raman (powder, cm^{-1}): 3374-3206 (N-H), 3077, 3051 (C-$H_{aromatic}$), 2940, 2954 (C-$H_{aliphatic}$), 1677, 1671 (C=O), 1598, 1593 (C=C), 1262-1147 cm^{-1} (C=S), 484, 477 (Fe-Cp); ^{1}H-NMR (500 MHz, DMSO-d_6, ppm) δ 12.18 (s, 1H, NH), 11.53 (s, 1H, NH), 7.94-7.39 (m, 7H, ArH), 4.58 (s, 2H, C_5H_4), 4.26 (s, 2H, C_5H_4), 4.08 (s, 5H, C_5H_5), 3.67 (s, 3H, OCH_3); ^{13}C-NMR (125.81 MHz, DMSO-d_6, ppm) δ 180.2, 166.4, 141.5, 138.9, 136.4, 134.6, 132.2, 130.6, 128.3, 125.7, 122.5, 118.2, 86.8, 70.5, 69.7, 68.9, 57.7; Elemental anal. Calcd. (%) for $C_{25}H_{21}BrFeN_2O_2S$: C, 54.64; H, 3.91; N, 5.13; S, 5.89; Fe, 10.19. Found (%): C, 54.57; H, 3.82; N, 5.20; S, 5.95; Fe, 10.12.

2.2.9 1-(4-bromobenzoyl)-3-(4-methoxy-3-ferrocenylphenyl)thiourea **(M9)**

Quantities used were 2.92 g (10 mmol) 4-methoxy-3-ferrocenylaniline, 0.98 g (10 mmol) potassium thiocyanate, and 1.32 ml (10 mmol) of 4-bromobenzoyl chloride. Yield 75%; Orange solid; m.p. 186 °C; FT-IR and Raman (powder, cm^{-1}): 3386-3209 (N-H), 3067, 3044 (C-$H_{aromatic}$), 2936, 2948 (C-$H_{aliphatic}$), 1667, 1661 (C=O), 1592, 1602 (C=C), 1255-1139 cm^{-1} (C=S), 482, 485 (Fe-Cp); ^{1}H-NMR (500 MHz, DMSO-d_6, ppm) δ 12.47 (s, 1H, NH), 11.74 (s, 1H, NH), 7.90-7.42 (m, 7H, ArH), 4.68 (s, 2H, C_5H_4), 4.36 (s, 2H, C_5H_4), 4.17 (s, 5H, C_5H_5), 3.79 (s, 3H, OCH_3); ^{13}C-NMR (125.81 MHz, DMSO-d_6, ppm) δ 178.8, 167.7, 140.1, 137.5, 135.8, 132.6, 130.5, 128.9, 125.6, 122.8, 120.7, 118.5, 86.9, 70.7, 69.8, 67.6, 53.8; Elemental anal. Calcd. (%) for $C_{25}H_{21}BrFeN_2O_2S$: C, 54.64; H, 3.91; N, 5.13; S, 5.89; Fe, 10.19. Found (%): C, 54.69; H, 3.96; N, 5.05; S, 5.77; Fe, 10.29.

2.3 DNA binding studies

2.3.1 Cyclic voltammetry

Voltammetric experiments were performed using a Biologic SP-300 voltammeter running on EC-Lab Express V 5.40 software, Japan. Analytical grade TBAP (Tertiarybutyl

View Article Online
DOI: 10.1039/C8NJ00483H

ammonium perchlorate) was used as supporting electrolyte and N_2 gas (99.9 %) was purged through the mixture to avoid any interference from oxygen. Commercial salmon sperm DNA (SS-DNA) obtained from Sigma Aldrich (Cat. No. 74782) was solubilized in doubly distilled water to prepare a stock solution of 6 x 10^{-4} M from which working concentrations of DNA were prepared. The concentration of the stock solution was measured by UV absorbance at 260 nm using an epsilon value of 6600 M^{-1} cm^{-1}. This DNA was protein free because A_{260}/A_{280} > 1.8. For electrochemical measurements, a known concentration of the test solution was kept in an electrochemical cell and the voltammogram was recorded in the absence of DNA. The procedure was then repeated for systems with a constant concentration of the drug and varying concentrations of DNA. The working electrode was polished with alumina powder and rinsed with distilled water before each measurement.[29]

2.3.2 UV-Vis spectrophotometry

Absorption spectra were recorded on a Shimadzu 1800 UV-Vis spectrophotometer. The absorption spectrum of a known concentration of the drug was recorded without DNA. The spectroscopic response was then monitored for the same amount of drug on addition of small aliquots of DNA solution. All samples were allowed to equilibrate for 15 min prior to each spectroscopic measurement.[29] Based on the variation in absorption maxima (λ_{max}) in the presence of DNA, the binding constant "*K*" of drug-DNA complex was calculated using the Benesi-Hildebrand equation:[30]

$$\frac{A_o}{A-A_o} = \frac{\varepsilon_G}{\varepsilon_{H-G}-\varepsilon_G} + \frac{\varepsilon_G}{\varepsilon_{H-G}-\varepsilon_G}\frac{1}{K[DNA]} \qquad \text{Eq 1}$$

where A_o and A are the absorbance of the free compound and of the compound-DNA complex, ε_G and $\varepsilon_{H\text{-}G}$ corresponds to the molar extinction coefficient of the free drug, and the extinction coefficient of the drug in the fully bound form, respectively.[31]

2.4 DFT calculations

Computational studies were carried out in order to calculate the energies of the frontier molecular orbitals (E_{HOMO} and E_{LUMO}), vibrational frequencies, and the Mulliken charge distribution on the molecular structures using the DFT/B3LYP method combined with 6-31G(d,p) basis set in DMSO. The density functional theory (DFT) was used because of its simplicity and less time consumption compared to more sophisticated calculations.[32] The

View Article Online
DOI: 10.1039/C8NJ00483H

structures of the molecules were first optimized using DFT and then energy calculations were performed on the optimized structures. Gaussian 03W software was used for calculations.

2.5 Antimicrobial assay

2.5.1 Antibacterial study

Antibacterial activities of the synthesized ferrocenyl compounds were determined against five representative, gram-positive (*S. aureus, S. typhimurium, M. luteus*) and gram-negative (*B. bronchiseptica and E. aerogenes*) bacterial strains, by the disc diffusion method.[33,34] Prior to use, the bacterial isolates under investigation were first cultured in a nutrient broth for 18 h and standardized to 0.5 McFarland turbidity scale (106 cfu mL^{-1}). The nutrient agar medium, which was prepared by adding 2.3 g nutrient agar (Merck) to 100 mL distilled water at pH 7.0, was autoclaved and then cooled down to 45 ^{o}C and seeded. Petri dishes in triplicate were prepared by introducing 75 mL of seeded nutrient agar medium and allowed to solidify. Wells were bored into the agar using a sterile 6 mm diameter cork borer. Approximately, 100 µL of the test compounds were infused into the wells, which were permitted to stand at room temperature for about 2 h and then incubated at 37 ^{o}C. Controls were set in parallel in which the respective solvents were used to fill the well. Subsequent to the incubation of plates at 37 ^{o}C for 24 h, the diameter of zone of inhibition was measured. The effects were compared with penicillin (positive control) at a concentration of 1.0 mg/mL. The relative percentage inhibition of the tested compounds with respect to positive control was calculated by using the following formula:

$$\text{Relative percentage inhibition of the test compound} = 100 \times (X-Y)/(Z-Y) \quad \text{Eq 2}$$

where X is the total area of inhibition of the test sample, Y is the total area of inhibition of the solvent and Z is the total area of inhibition of the standard drug.

2.5.2 Antifungal study

The sensitivity of the synthesized complexes was tested against three different fungal strains, namely *F. moniliforme, A. fumigatus* and *A. flavus* using the agar tube dilution method.[33,34] Sample preparation was done by dissolving 2 mg of the compound in 1.0 mL of DMSO. In order to prepare the culture media, 6.5 g of sabouraud dextrose agar was dissolved in 100 mL distilled water (pH = 5.6). Next, 10 mL of the sabouraud dextrose agar (Merck) was introduced into screw-capped tubes or cotton-plugged test tubes and autoclaved at 121

View Article Online
DOI: 10.1039/C8NJ00483H

°C for 21 min. The tubes were cooled to 50 °C and sabouraud dextrose agar was loaded with 70 µL of the compound taken from stock solution. The tubes containing the media were then solidified in a slanting position at room temperature. For each fungal strain, three slants of test compound were prepared. Tubes comprising the solidified media and test compounds were infused with a 4-mm diameter piece of inoculum, taken from a 7-day old culture of fungus. One test tube of each compound was prepared, which was used for positive control. Slants without compound were used for negative control. The test tubes were incubated at 28 °C for 7 days. During incubation, the cultures were examined twice a week. Readings were taken by measuring the linear length (mm) of the fungus in slant and growth inhibition was calculated with reference to the control. Percentage inhibition of fungal growth for each concentration of the compound was determined by using following formula:

$$\text{Percentage inhibition of fungal growth} = 100 - \frac{\text{Linear growth in test (cm)}}{\text{Linear growth in control (cm)}} \times 100 \qquad \text{Eq 3}$$

2.6 Cytotoxic screening

The growth inhibitory effect of the synthesized complexes on human breast cancer cell line MCF-7 (ATCC# HTB-22), and breast non-cancerous cells MCF-10A (ATCC# CRL-10317) was assessed by use of the MTT (3-(4,5-dimethylthiazol-2-yl)-2,5-diphenyl tetrazolium bromide) assay, in which the metabolically active cells reduce MTT to yield a DMSO soluble formazan product that can be analyzed calorimetrically.[35,36] The cells were maintained and cultured in RPMI 1640 culture medium supplemented with 10% FBS (fetal bovine serum). Cisplatin was used as a control. In brief, 1 x 10^4 cells were seeded in triplicate into the wells of the flat bottomed 96-well culture plates. The plates were incubated at 37 °C for 24 h in a humidified atmosphere (5% carbon dioxide in air, pH 7.4) to permit the cells to attach. The samples were then added at different concentrations (0-100 µM) to triplicate wells. After 72 h of incubation, the cells were exposed to 20 µL of MTT (5 mg/mL) and incubated for 4 h at 37 °C for further cultivation. The yellow formazan crystals thus produced in each well were solubilized in 200 µL of DMSO and the absorbance of the resulting solution was read at 570 nm using a microplate reader (Labsystems Multiskan MS). The sensitivity of the compounds **M1-M9** against the subjected cell lines was expressed in terms of IC_{50} values (drug concentration that resulted in 50% reduction of cell growth), calculated on the regression line where the absorbance values at 570 nm were plotted against logarithm of drug concentration. The experiment was performed in triplicate.

View Article Online
DOI: 10.1039/C8NJ00483H

3. Results and discussion

3.1 Chemistry and spectroscopic study

The synthesis of ferrocene-containing acyl thioureas **(M1-M9)** was accomplished by allowing the ferrocenyl anilines to react with freshly prepared isothiocyanates under an inert (N_2) atmosphere in dry acetone (Scheme 1).

The FT-IR and Raman spectra of the compounds **M1-M9** indicated that the main vibrational stretching modes were observed between 3392-3204 (N-H), 3091-3025 (C-$H_{aromatic}$), 2954-2926 (C-$H_{aliphatic}$), 1677-1663 (C=O), 1602-1587 (C=C), 1268-1125 cm^{-1} (C=S), and 488-473 (Fe-Cp), respectively. The disappearance of the characteristic band for isothiocyanate (N=C=S) in the region of 2000 cm^{-1} and the appearance of a thiocarbonyl (C=S) band in the range of 1300-1100 cm^{-1} confirms the formation of thioureas **(M1-M9)**, as a result of coupling of 4-methoxy-3-ferrocenylaniline with freshly prepared isothiocyanates. A broad signal between 3392-3204 cm^{-1} due to the N-H stretch is attributable to intra- and intermolecular hydrogen bonding. The carbonyl group appeared as an intense band at 1676-1661 cm^{-1}, while all the other bands are evident in their normal characteristic regions.

The ^{1}H-NMR data for the synthesized thioureas **(M1-M9)** indicate that the –NH hydrogen resonates considerably downfield from other resonances in the spectra at around 12.75-12.18 and 11.74-11.06 ppm. In most cases, the formation of thioureas results in slight downfield chemical shifts of the aromatic and ferrocenyl protons compared to 4-methoxy-3-ferrocenyl aniline**,** which is obvious as the neighboring thiocarbonyl moiety is also attracting electron density. The ^{1}H-NMR spectra show that the unsubstituted cyclopentadienyl (η^5-C_5H_5) ring of ferrocene yielded an intense singlet at ~4 ppm. In the case of substituted (η^5-C_5H_4) ring, the *ortho* protons appear in the region of 4.77-4.58 ppm, while the *meta* protons occur in the range of 4.45-4.26 ppm. Aromatic protons were visible between 8-7 ppm. The ^{13}C-NMR spectral data also justifies the coupling of ferrocenyl aniline with respective isothiocyanates yielding the ferrocene incorporated acyl thioureas **(M1-M9)**. The chemical shifts of the carbons of the CSNH and CONH groups of the thioureas resonate around 180.2-177.1 and 169.7-165.4 ppm, respectively.

Elemental analyses (CHNS) of all the compounds showed that the calculated and found values for carbon, hydrogen, nitrogen, and iron are in good agreement with each other, which establishes that the compounds are amply pure in bulk.

View Article Online
DOI: 10.1039/C8NJ00483H

3.2 DNA binding studies

3.2.1 Cyclic voltammetry (CV)

A cyclic voltammetric study was executed with the aim of understanding the redox behavior and the DNA binding affinities of the synthesized compounds. Electrochemical measurements were undertaken using a three-electrode system, i.e., working (platinum disc electrode with a geometric area of 0.071 cm^2), reference (saturated calomel electrode i.e. SCE) and auxiliary electrodes (platinum electrode with geometric area much greater than the working electrode). Variation in the peak current provided information about the DNA binding constants, whereas the mode of interaction of compound with DNA can be judged from the shift in the peak potential. Drug-DNA binding constants were determined with the help of following equation:[37]

$$\log (1/[DNA]) = \log K + \log \{I/(I_o - I)\} \quad \text{Eq 5}$$

where K is the binding constant, I and I_o are the peak currents with and without DNA. For the determination of binding site size the following equation was used:[38]

$$C_b/C_f = K\,[\text{free base pairs}]/s \quad \text{Eq 6}$$

where s is the binding site size in terms of base pair, K is the binding constant, C_f represents the concentration of free species and C_b denotes the concentration of drug-DNA bound species. Considering the concentration of DNA in terms of nucleotide phosphate, the concentration of DNA base pair will be taken as [DNA base pair]/2 and Eq 6 can be written as:[37]

$$C_b/C_f = K\,[\text{DNA base pairs}]/2s \quad \text{Eq 7}$$

and the value of C_b/C_f is equal to $(I_o\text{-}I)/I$, which are the values of experimental peak currents. The diffusion coefficient of free drug and DNA-bound drug provides the best information about the molecular mass of the drug-DNA adduct. The following form of the Randles-Sevcik equation was used for calculating the diffusion coefficients:[39,40]

$$I_{pa} = 2.99 \times 10^5\, n\,(\alpha n)^{1/2} A\, C_o^*\, D_o^{1/2}\, \upsilon^{1/2} \quad \text{Eq 8}$$

View Article Online
DOI: 10.1039/C8NJ00483H

where I_{pa} is the anodic peak current, C_o^* is the concentration of the reductant in mol L^{-1}, A is the geometric area of the electrode in cm^2, υ is the scan rate in V/s, α is the transfer coefficient, n is the number of electrons involved in the process, D_o is the diffusion coefficient in $cm^2\ s^{-1}$.

The synthesized ferrocene-based compounds display similar electrochemical behavior with two well-defined and stable redox peaks in the potential range of -0.2-1.0 V. Figure 1 shows the DNA binding study of a representative compound **(M3)** with CV. The consistency of the voltage at different scan rates from the plots of current (mA) *vs*. potential (E/V *vs*. SCE) for the compound favors a quasi-reversible electrochemical process (Figure 1a). The voltammogram of **M3** indicates an oxidation maximum at 0.377 V and a reduction maximum at 0.253 V. With the addition of 3-12 μM DNA, a negative shift in the peak potential and a decay in the peak current is observed. This negative shift in potential justifies the probability of an electrostatic mode of interaction of the positively charged **M3** with the anionic phosphate backbone of DNA. The decrease in current is attributed to the formation of a high molecular weight M**3**-DNA adduct, which diffuses comparatively slowly, thus causing a reduction in peak current (Figure 1b). The diffusion coefficient of **M3**-DNA adduct is 4.53 x 10^{-7} $cm^2\ s^{-1}$, and this is far less than the diffusion coefficient of the free **M3** (6.66 x 10^{-7} $cm^2\ s^{-1}$). This result indicates the slow diffusion of the high molecular weight **M3**-DNA adduct as compared to the free **M3** (Figure 1c). The binding constant (5.713 x 10^4 M^{-1}), and binding site size (0.532 bp) were calculated using Eqs. 5 and 6, respectively (Figure 1d and 1e).

View Article Online
DOI: 10.1039/C8NJ00483H

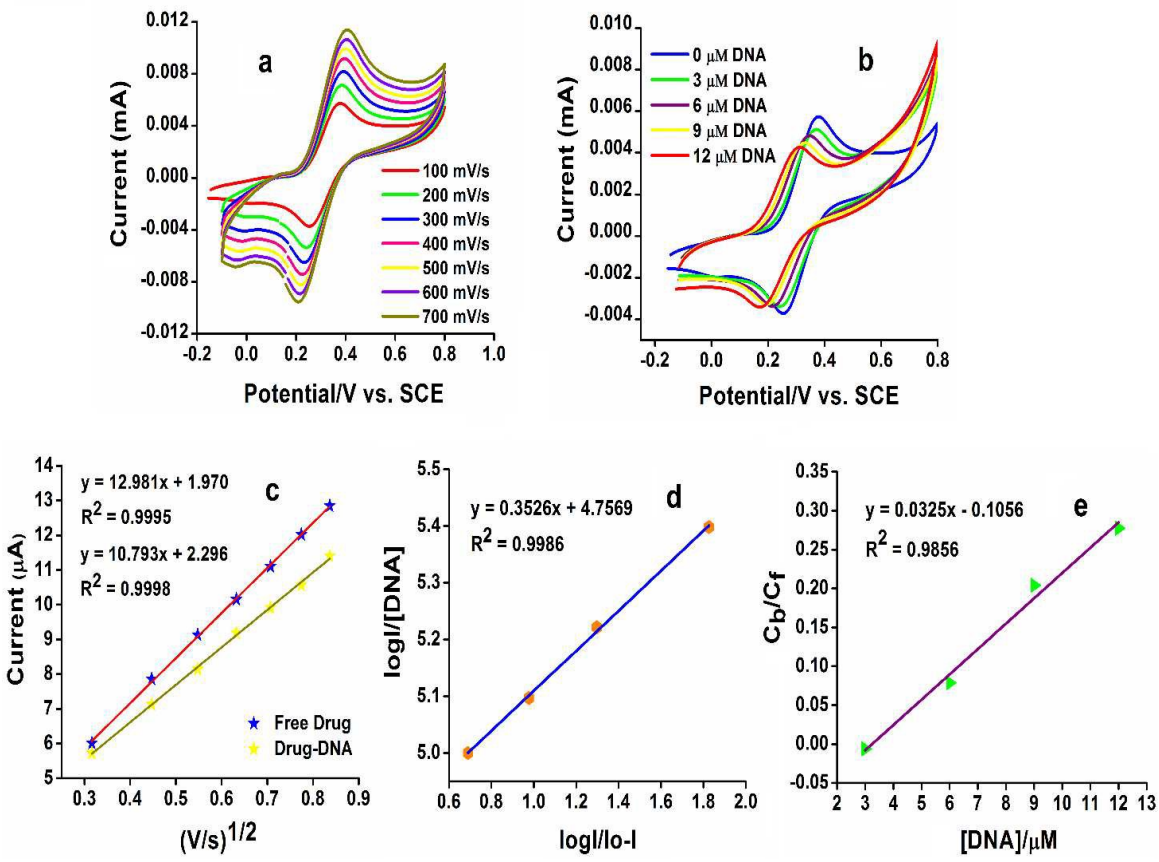

Figure 1. (a) Representative plots of Current *vs*. Potential/V (SCE) at different scan rates for **M3**. (b) Cyclic voltammogram of 1 mM **M3** with 1 mL of 0.5 M TBAP as supporting electrolyte in the absence and presence of 3-12 μM DNA showing a decrease in I from I_o and a concentration dependent -ve shift in potential showing electrostatic interactions. (c) Representative plot of current *vs*. $(V/s)^{1/2}$, for the determination of diffusion coefficient of free **M3** and **M3**-3 μM DNA. (d) Representative plot of log (I/I_o-I) *vs*. log (1/[DNA] for determination of binding constant of **M3**. (e) Plot of C_b/C_f *vs*. [DNA]/μM for determination of binding site size of 3-12 μM DNA concentrations **M3**.

The important DNA binding parameters of the compounds studied are listed in Table 1. These binding constant values are far better than protonated ferrocene (3.45×10^2 M^{-1}) and are comparable with many of the recently reported ferrocene derivatives,[40-43] which shows that the thiourea moiety is playing its part in the enhancement of binding constant. The synthesized ferrocenyl derivatives are believed to undergo electrostatic interaction of positively charged ferrocenium state with the negatively charged oxygen of DNA. The phenyl group present in the structure is also capable of forming π-H bonding (π-stacking) with DNA bases. This may be due to the existence of amide in the structure that could

View Article Online
DOI: 10.1039/C8NJ00483H

interact with DNA bases *via* hydrogen-bonding, as previously reported for benzamides,[44] ferrocenyl urea, thiourea and guanidine derivatives.[45,46]

Table 1. Important parameters for redox behavior and DNA binding studies (CV and UV).

	CV				UV
Code	**Binding Constant K [M^{-1}]**	**D_o [cm^2s^{-1}] Free drug**	**Do [cm^2s^{-1}] drug-DNA**	**Binding site size 's' [bp]**	**Binding Constant K [M^{-1}]**
M1	4.87×10^4	1.48×10^{-7}	1.03×10^{-7}	0.505	4.93×10^4
M2	4.25×10^4	3.43×10^{-7}	2.84×10^{-7}	0.338	3.27×10^4
M3	5.71×10^4	6.66×10^{-7}	4.53×10^{-7}	0.532	5.00×10^4
M4	3.84×10^4	5.25×10^{-7}	2.44×10^{-7}	0.303	3.15×10^4
M5	2.92×10^4	6.87×10^{-7}	4.13×10^{-7}	0.278	3.07×10^4
M6	2.21×10^4	2.67×10^{-7}	1.67×10^{-7}	0.217	2.58×10^4
M7	1.93×10^4	5.26×10^{-7}	3.58×10^{-7}	0.196	2.26×10^4
M8	9.75×10^3	4.28×10^{-7}	2.03×10^{-7}	0.105	1.04×10^4
M9	1.36×10^4	7.94×10^{-7}	4.41×10^{-7}	0.177	1.98×10^4

3.2.2 UV-Vis spectroscopy

The results obtained from CV were equally supported by UV-Vis spectroscopy confirming the electrostatic interactions of the compounds with DNA. The characteristic UV spectrum of the compound **M3** gave two peaks in the UV region. One at 244 nm is due to a π-π* transition in the cyclopentadienyl ring (Cp) of ferrocene and the other at 286 nm is attributed to the π-π* transition of electrons in the phenyl chromophore. Following the substantial addition of DNA, the UV-Vis spectra of the compounds showed a decrease in absorption with a slight blue shift (hypochromism) (Figure 2a). The hypochromic effect is thought to be due to the interaction between the electronic states of the binding chromophore and those of the DNA bases.[29,47] It is likely that the strength of this electronic interaction would decline as the cube of the distance of separation between the chromophore and the DNA bases.[48] So, the noticeable hypochromism observed in our experiments proposed the close vicinity of the chromophore of synthesized complexes to the DNA bases. At the closest approach to DNA, the π* orbital of the binding moiety of compounds could couple with π

View Article Online
DOI: 10.1039/C8NJ00483H

orbital of purine or pyrimidine. The coupling π* orbital may get partially filled by electrons, thus decreasing the transition probabilities, and hence result in hypochromism.[49,50] A binding constant of 5.004 x 10^4 M^{-1} for **M3** was determined from the Figure 2b.

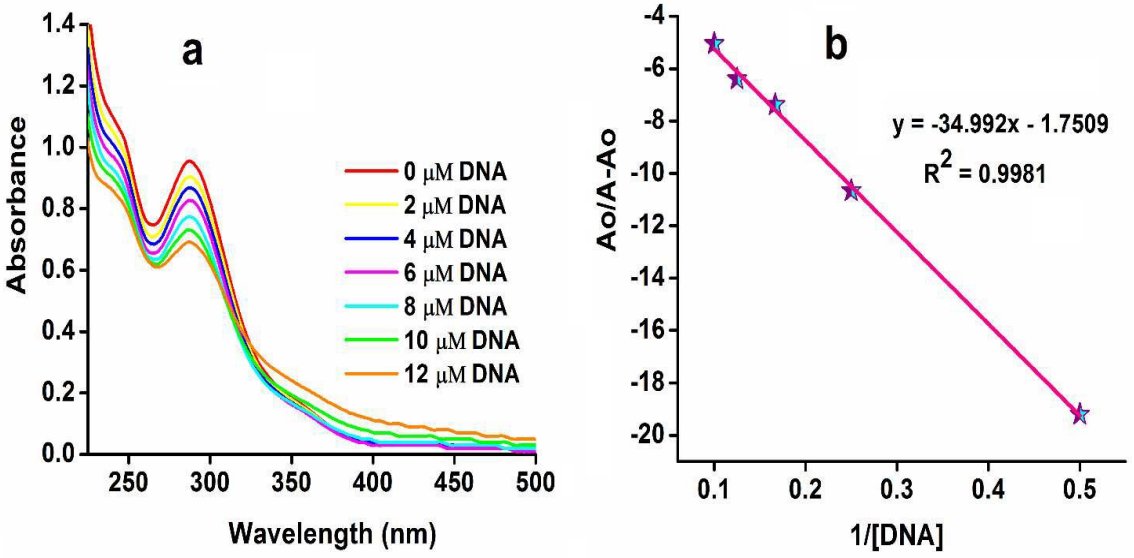

Figure 2. (a) Representative plots of absorbance *vs*. wavelength of 25 μM **M3** in ethanol with increasing concentration of DNA (2-12 μM). (b) Plot of $A_o/A\text{-}A_o$ *vs*. 1/[DNA] for determination of DNA binding constant of **M3**.

3.3 DFT study

Computational calculations were performed for these electroactive compounds in order to complement the experimental outcomes of cyclic voltammetry and infra-red spectroscopy. The redox potentials of the compounds measured from cyclic voltammetry revealed an analogous trend to that anticipated from the DFT work.

Figure 3a and 3b shows the representative graphical demonstration of the HOMO and LUMO orbitals of **M3**. The HOMO orbitals are localized on the ferrocene moiety (Fe metal), whereas, the LUMO orbitals are extended over the thiourea functionality (containing electron withdrawing N, and O atoms), and the fluoro-substituted phenyl ring. Generally, the energy values of HOMO/LUMO and their energy gap reflect the chemical activity of the molecule. The HOMO orbitals indicate the preferred site for the oxidation of electroactive species, whereas the LUMO orbitals correspond to the probable site for the reduction of optimized compound. HOMO as an electron donor represents the ability to donate an electron, while LUMO as an electron acceptor indicates the ability to receive an electron.[51,52] The HOMO-

View Article Online
DOI: 10.1039/C8NJ00483H

LUMO energy gap reveals the intramolecular charge transfer (ICT) interaction occurs within the molecule.

The ease of reduction of the compounds was found to vary as: **M3 > M1 > M2 > M4 > M5 > M6 > M7 > M9 > M8**. A similar trend was acquired from the E_{LUMO} values, i.e., the highest reduction potential and most negative E_{LUMO} value of **M3** corresponds to easiest reduction.[53-55] A more negative E_{LUMO} favors addition of electrons as the energies of the orbitals are reduced.

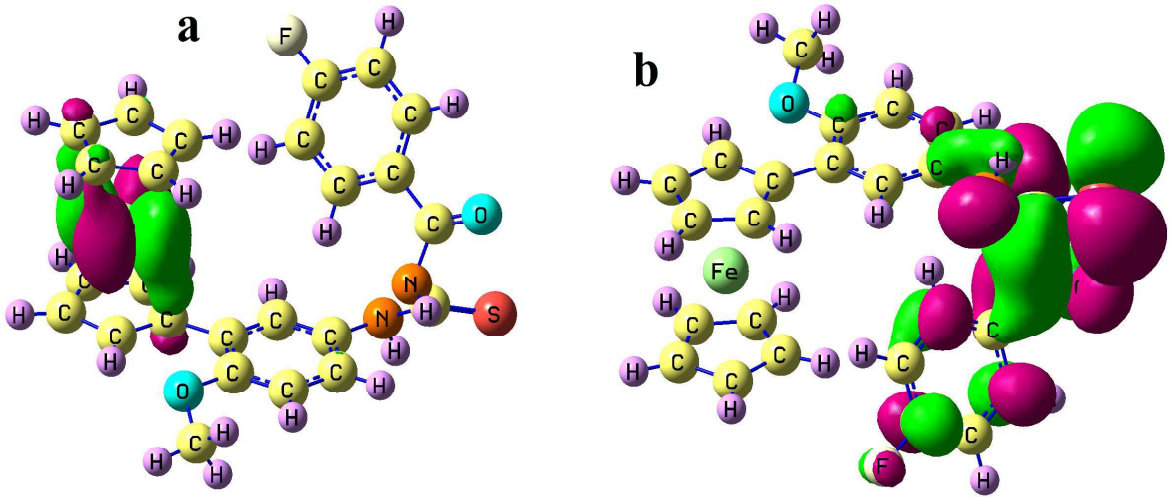

Figure 3. (a) Representative graphical demonstration of HOMO of **M3**. (b) Representative graphical representation of LUMO of **M3**.

The E_{HOMO} values acquired from DFT were compared with the oxidation potentials obtained from the CV measurements. The oxidation potentials observed experimentally for compounds **M1-M9** fluctuate as: **M8 > M9 > M7 > M6 > M5 > M4 > M2 > M1 > M3**. This observation is supported from the DFT study by comparing the E_{HOMO} values, which is less negative for **M8**, representing its ease of oxidation as compared to other compounds (Figure 4 and Table 2). The HOMO-LUMO energy gaps were observed to be in close agreement with the electrochemical band gaps (correlation coefficient = 0.953), computed from the difference between the oxidation and reduction potential of the species ($E_{redox} = E_{oxi} - E_{red}$) (Table 2 and Figure 5).

DFT-based measurements also facilitated us to ascertain the Mulliken charges on these molecular structures to determine the sites which are prone to electrophilic or nucleophilic attack.[56] Figure 6a and 6b demonstrates the graphical description of Mulliken

View Article Online
DOI: 10.1039/C8NJ00483H

charge distribution on the representative compound **M3**. The investigated molecule **M3** has several possible sites for electrophilic (the electrophilic sites are most electronegative and are represented as red color), and nucleophilic attack (the nucleophilic sites are most positive and are represented as green color).

Table 2. E_{HOMO} and E_{LUMO} values obtained through DFT calculations.

Sample Code	E_{HOMO} (eV)	E_{LUMO} (eV)	HOMO-LUMO Band Gap (eV)	Electrochemical Band Gap (V)
M1	-0.4365	-0.3341	0.1024	0.1296
M2	-0.4129	-0.3022	0.1107	0.1331
M3	-0.4586	-0.3657	0.0929	0.1260
M4	-0.3903	-0.2715	0.1188	0.1384
M5	-0.3561	-0.2304	0.1257	0.1432
M6	-0.3216	-0.1823	0.1323	0.1489
M7	-0.3025	-0.1637	0.1388	0.1552
M8	-0.2572	-0.1029	0.1543	0.1736
M9	-0.2686	-0.1230	0.1456	0.1608

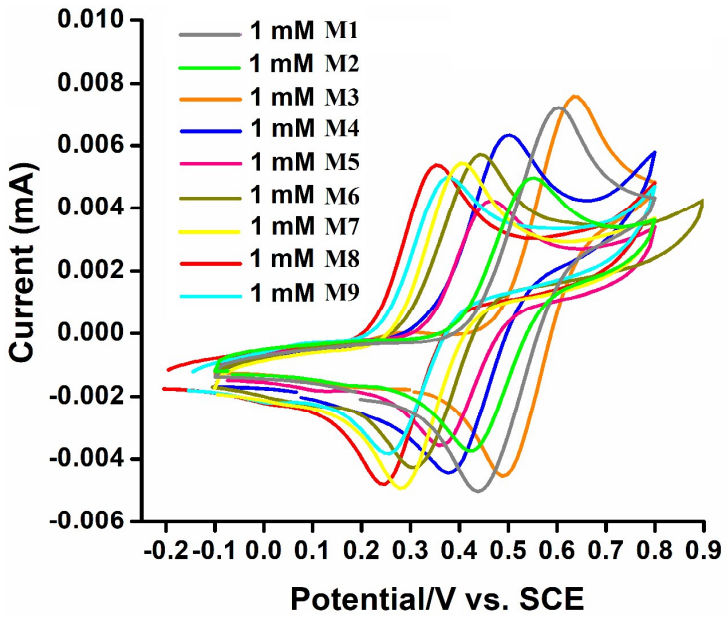

Figure 4. Comparison of oxidation and reduction potentials of 1 mM ferrocenyl thioureas **M1-M9** in DMSO recorded at a scan rate of 200 mV/s.

View Article Online
DOI: 10.1039/C8NJ00483H

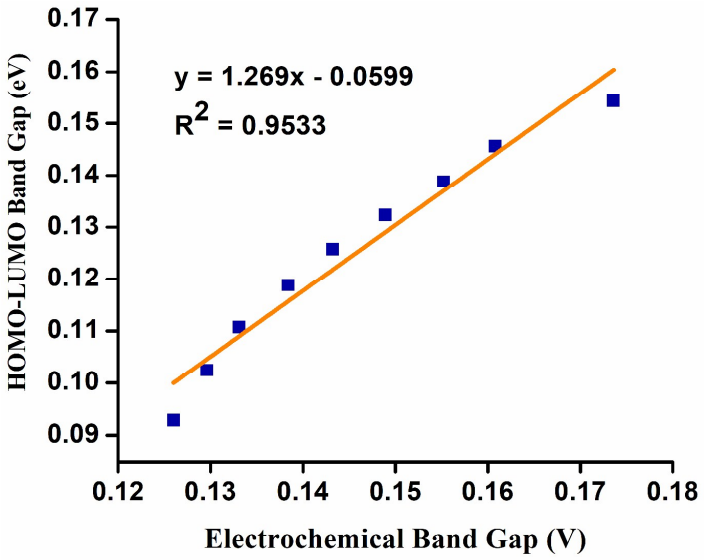

Figure 5. Linear correlation graph between electrochemical band gap and HOMO-LUMO band gap. (Correlation coefficient = 0.953)

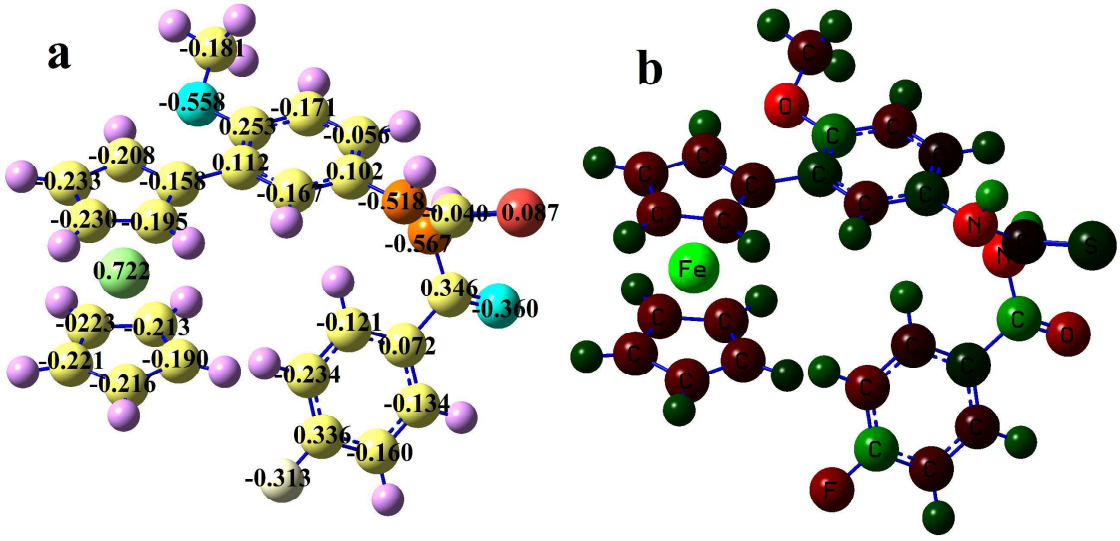

Figure 6. (a) Graphical representation of Mulliken charges on the molecular structure **M3** (by numbers). (b) Mulliken charge distribution on the optimized molecule **M3** designated by color change on the atoms (red for negative charge and blue for positive charge).

The vibrational frequencies determined experimentally are compared with those obtained theoretically from DFT calculations employing the B3LYP/6-31G(d,p) method for the optimized geometry of the compounds **(M1-M9)**. Some important calculated and experimental vibrational frequencies along with their vibrational assignments are listed in Table 3. Vibrational frequencies were scaled by the typical factor 0.96. The theoretical

View Article Online
DOI: 10.1039/C8NJ00483H

vibrational frequencies and the observed spectroscopic data illustrate a linear relationship as presented in the Figure 7 (correlation coefficient = 0.994). The largest difference between the calculated and observed frequencies is 20 cm^{-1}. The experimental and calculated IR spectra for **M3** are shown in Figure S1 and S2 (ESI file).

Table 3. Vibrational frequencies (for selected vibrations only) of ferrocenyl thioureas **(M1-M9)** calculated at the B3LYP/6-31G(d,p) level compared with the experimental data.

	Calculated and Experimental IR Vibrational Frequencies (cm^{-1})								
Assignment	**M1**	**M2**	**M3**	**M4**	**M5**	**M6**	**M7**	**M8**	**M9**
υ N-H	3379-3215 (Cal)	3348-3197 (Cal)	3395-3287 (Cal)	3375-3226 (Cal)	3352-3219 (Cal)	3380-3206 (Cal)	3397-3231 (Cal)	3389-3216 (Cal)	3364-3225 (Cal)
	3392-3227 (Exp)	3360-3217 (Exp)	3374-3233 (Exp)	3388-3212 (Exp)	3364-3204 (Exp)	3391-3223 (Exp)	3382-3219 (Exp)	3374-3206 (Exp)	3386-3209 (Exp)
υ $C-H_{aromatic}$	3038 (Cal)	3056 (Cal)	3071 (Cal)	3060 (Cal)	3072 (Cal)	3069 (Cal)	3047 (Cal)	3093 (Cal)	3082 (Cal)
	3025 (Exp)	3074 (Exp)	3086 (Exp)	3076 (Exp)	3088 (Exp)	3055 (Exp)	3064 (Exp)	3077 (Exp)	3067 (Exp)
υ $C-H_{aliphatic}$	2962 (Cal)	2954 (Cal)	2948 (Cal)	2940 (Cal)	2970 (Cal)	2937 (Cal)	2965 (Cal)	2932 (Cal)	2951 (Cal)
	2946 (Exp)	2935 (Exp)	2931 (Exp)	2927 (Exp)	2951 (Exp)	2949 (Exp)	2944 (Exp)	2940 (Exp)	2936 (Exp)
υ C=O	1674 (Cal)	1652 (Cal)	1664 (Cal)	1675 (Cal)	1660 (Cal)	1657 (Cal)	1663 (Cal)	1668 (Cal)	1655 (Cal)
	1663 (Exp)	1665 (Exp)	1676 (Exp)	1668 (Exp)	1672 (Exp)	1669 (Exp)	1674 (Exp)	1677 (Exp)	1667 (Exp)
υ C=C	1609 (Cal)	1598 (Cal)	1603 (Cal)	1602 (Cal)	1599 (Cal)	1604 (Cal)	1601 (Cal)	1589 (Cal)	1597 (Cal)
	1602 (Exp)	1590 (Exp)	1591 (Exp)	1593 (Exp)	1595 (Exp)	1587 (Exp)	1594 (Exp)	1598 (Exp)	1592 (Exp)
β N-H	1567 (Cal)	1549 (Cal)	1563 (Cal)	1553 (Cal)	1545 (Cal)	1572 (Cal)	1547 (Cal)	1551 (Cal)	1542 (Cal)
	1553 (Exp)	1562 (Exp)	1546 (Exp)	1567 (Exp)	1560 (Exp)	1558 (Exp)	1564 (Exp)	1568 (Exp)	1557 (Exp)
δ $C-H_{aliphatic}$	1460 (Cal)	1449 (Cal)	1445 (Cal)	1438 (Cal)	1435 (Cal)	1447 (Cal)	1451 (Cal)	1440 (Cal)	1446 (Cal)
	1446 (Exp)	1438 (Exp)	1456 (Exp)	1453 (Exp)	1442 (Exp)	1458 (Exp)	1435 (Exp)	1449 (Exp)	1455 (Exp)

Cal = calculated frequency; Exp = experimental frequency; υ = stretching; δ = deformation; β = in-plane bending; γ = out of plane bending; ω = wagging; ρ = rocking.

View Article Online
DOI: 10.1039/C8NJ00483H

Table 3. Continued……

Calculated and Experimental IR Vibrational Frequencies (cm^{-1})									
Assignment	**M1**	**M2**	**M3**	**M4**	**M5**	**M6**	**M7**	**M8**	**M9**
υ C=S	1244-1131 (Cal)	1250-1135 (Cal)	1288-1190 (Cal)	1248-1125 (Cal)	1251-1128 (Cal)	1264-1142 (Cal)	1257-1149 (Cal)	1245-1124 (Cal)	1270-1150 (Cal)
	1257-1138 (Exp)	1261-1143 (Exp)	1268-1147 (Exp)	1265-1132 (Exp)	1260-1136 (Exp)	1253-1154 (Exp)	1266-1125 (Exp)	1262-1147 (Exp)	1255-1139 (Exp)
ω C-$H_{aliphatic}$	1064 (Cal)	1048 (Cal)	1046 (Cal)	1061 (Cal)	1046 (Cal)	1067 (Cal)	1063 (Cal)	1044 (Cal)	1050 (Cal)
	1052 (Exp)	1040 (Exp)	1068 (Exp)	1043 (Exp)	1058 (Exp)	1050 (Exp)	1054 (Exp)	1053 (Exp)	1061 (Exp)
ρ C-$H_{aliphatic}$	1010 (Cal)	1014 (Cal)	1012 (Cal)	1029 (Cal)	1015 (Cal)	1009 (Cal)	1028 (Cal)	1017 (Cal)	1012 (Cal)
	1023 (Exp)	1019 (Exp)	1025 (Exp)	1020 (Exp)	1027 (Exp)	1024 (Exp)	1013 (Exp)	1002 (Exp)	1025 (Exp)
β C-$H_{aromatic}$	980 (Cal)	985 (Cal)	973 (Cal)	989 (Cal)	981 (Cal)	962 (Cal)	977 (Cal)	958 (Cal)	990 (Cal)
	967 (Exp)	972 (Exp)	984 (Exp)	980 (Exp)	976 (Exp)	984 (Exp)	960 (Exp)	975 (Exp)	979 (Exp)
γ C-$H_{aromatic}$	856 (Cal)	840 (Cal)	831 (Cal)	863 (Cal)	850 (Cal)	853 (Cal)	860 (Cal)	851 (Cal)	867 (Cal)
	847 (Exp)	859 (Exp)	853 (Exp)	854 (Exp)	837 (Exp)	842 (Exp)	849 (Exp)	846 (Exp)	858 (Exp)
β C=O	795 (Cal)	777 (Cal)	786 (Cal)	798 (Cal)	792 (Cal)	776 (Cal)	785 (Cal)	791 (Cal)	785 (Cal)
	776 (Exp)	784 (Exp)	770 (Exp)	786 (Exp)	783 (Exp)	789 (Exp)	774 (Exp)	779 (Exp)	772 (Exp)
γ N-H	713 (Cal)	719 (Cal)	718 (Cal)	708 (Cal)	720 (Cal)	705 (Cal)	718 (Cal)	710 (Cal)	720 (Cal)
	704 (Exp)	711 (Exp)	723 (Exp)	717 (Exp)	712 (Exp)	716 (Exp)	701 (Exp)	721 (Exp)	725 (Exp)
γ C=O	638 (Cal)	630 (Cal)	644 (Cal)	648 (Cal)	645 (Cal)	633 (Cal)	636 (Cal)	630 (Cal)	644 (Cal)
	647 (Exp)	642 (Exp)	635 (Exp)	640 (Exp)	637 (Exp)	641 (Exp)	646 (Exp)	639 (Exp)	635(Exp)
υ Fe-Cp	471 (Cal)	485 (Cal)	482 (Cal)	487 (Cal)	472 (Cal)	475 (Cal)	473 (Cal)	468 (Cal)	470 (Cal)
	481 (Exp)	478 (Exp)	470 (Exp)	475 (Exp)	485 (Exp)	481 (Exp)	488 (Exp)	484 (Exp)	482 (Exp)

Cal = calculated frequency; Exp = experimental frequency; υ = stretching; δ = deformation; β = in-plane bending; γ = out of plane bending; ω = wagging; ρ = rocking.

View Article Online
DOI: 10.1039/C8NJ00483H

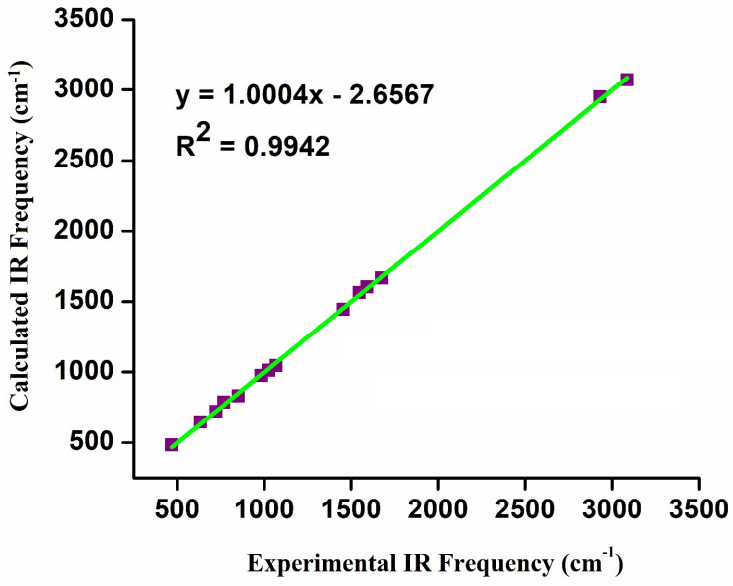

Figure 7. Linear correlation graph between the experimental and calculated vibrational frequencies of a representative compound **M3**. (Correlation coefficient = 0.994)

3.4 Antimicrobial studies

These compounds were subjected against representative bacterial and fungal strains and the results are summarized in Table 4 and 5, respectively. Penicillin and terbinafin were used as standard antimicrobial drugs and DMSO was selected as a negative control in order to determine its non-toxic effect. The zone of inhibition values represent the mean value of the three readings with standard deviation. The fluoro derivatives **M1**, **M2**, and **M3** showed more potent antimicrobial activity as compared to the chloro and bromo containing molecules. Moreover, the *ortho* substituted compounds were found to be biologically more active as compared to their *meta* and *para* derivatives, possibly due to the prominent effect of an electronegative group (X) at the *ortho* position than at the *meta* and *para* positions (inductive effect works up to three or four bonds). Due to electron withdrawing effect, a decrease in the basicity of NH and increase in lipophilicity may occur.[41] The decrease in basicity is due to less availability of the lone pair of electron to hydrogen bond with water in the living cells (Scheme 2a and 2b).

View Article Online
DOI: 10.1039/C8NJ00483H

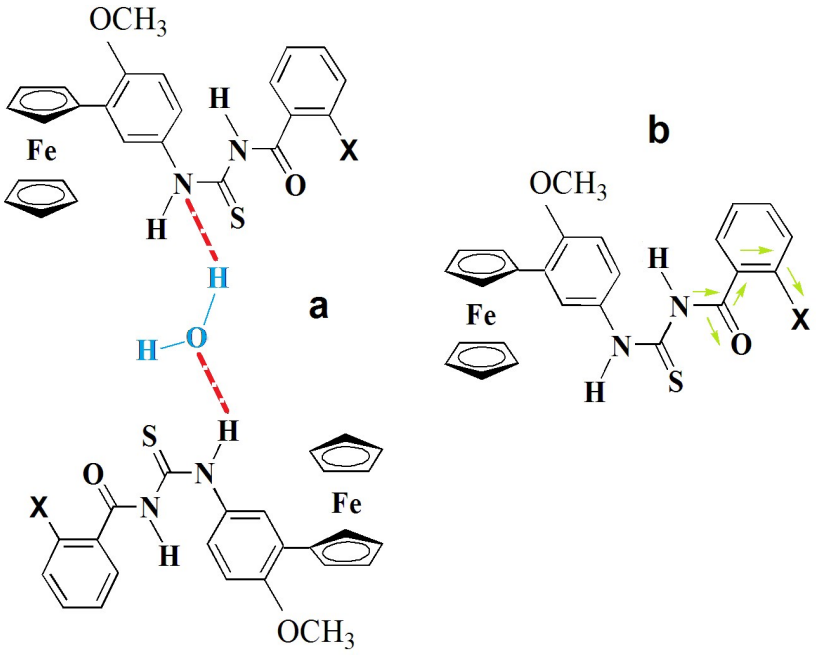

Scheme 2. (a) Hydrophilicity of ferrocenyl thioureas. (b) Decrease in hydrophilicity and increase in lipophilicity by an electron-withdrawing group (where X = F, Cl, and Br).

Table 4. *In vitro* antibacterial activity of synthesized ferrocenyl thioureas.

Sample Code	Staphylococcus aureus	Salmonella typhimurium	Micrococcus luteus	Bordetella bronchiseptica	Enterobacter aerogenes
M1	21.4 ± 0.33[a]	18.8 ± 0.67	20.2 ± 0.70	16.4 ± 0.30	16.0 ± 0.58
M2	18.6 ± 0.60	17.5 ± 0.30	18.3 ± 0.58	14.2 ± 0.70	14.9 ± 0.33
M3	19.5 ± 0.45	18.0 ± 0.44	18.9 ± 0.33	15.3 ± 0.58	15.8 ± 0.67
M4	18.1 ± 0.67	17.3 ± 0.37	16.5 ± 0.67	13.7 ± 0.55	14.0 ± 0.44
M5	17.5 ± 0.33	16.8 ± 0.53	15.7 ± 0.30	13.2 ± 0.65	13.4 ± 0.57
M6	17.0 ± 0.60	16.2 ± 0.70	14.9 ± 0.33	12.6 ± 0.45	12.5 ± 0.60
M7	16.4 ± 0.77	15.6 ± 0.63	14.2 ± 0.72	12.0 ± 0.60	11.6 ± 0.73
M8	14.7 ± 0.30	14.4 ± 0.33	13.0 ± 0.55	10.8 ± 0.77	09.9 ± 0.58
M9	15.8 ± 0.45	15.1 ± 0.77	13.6 ± 0.58	11.3 ± 0.33	10.5 ± 0.33
PC	26.7 ± 0.33	26.3 ± 0.33	27.3 ± 0.33	23.0 ± 0.58	20.3 ± 0.67

PC = Penicillin (1 mg/mL) was used as standard drug (positive control), while DMSO was used as negative control.

[a] Zone of inhibition in mm.

View Article Online
DOI: 10.1039/C8NJ00483H

Table 5. *In vitro* antifungal assay of synthesized ferrocenyl derivatives and the standard drug.

Sample Code	Fusarium moniliforme		Aspergillus fumigatus		Aspergillus flavus	
M1	3.46 ± 0.03[a]	64[b]	3.55 ± 0.33	66	2.97 ± 0.33	72
M2	3.78 ± 0.07	67	3.84 ± 0.06	63	2.25 ± 0.03	79
M3	2.65 ± 0.33	75	2.89 ± 0.09	73	1.57 ± 0.07	86
M4	4.35 ± 0.03	57	4.21 ± 0.33	59	3.29 ± 0.33	68
M5	5.53 ± 0.33	46	5.50 ± 0.07	55	4.27 ± 0.06	56
M6	4.69 ± 0.09	53	5.04 ± 0.63	50	4.15 ± 0.09	60
M7	5.96 ± 0.03	42	5.45 ± 0.09	47	4.59 ± 0.33	54
M8	3.17 ± 0.70	30	6.19 ± 0.67	40	5.17 ± 0.03	49
M9	7.94 ± 0.09	23	6.85 ± 0.33	33	5.85 ± 0.67	43
PC	0.77 ± 0.07	92	0.89 ± 0.03	92	0.83 ± 0.01	92
NC	10.3 ± 0.3	0	10.7 ± 0.03	0	10.3 ± 0.3	0

PC = Terbinafin (1 mg/ml) was used as standard drug (positive control), while DMSO was used as negative control (NC).
[a] Fungal growth (cm)
[b] Zone of inhibition (%)

3.5 Cytotoxicity assay

The anticancer activity of the synthesized complexes along with that for cisplatin (used as control) were assessed against MCF-7 carcinoma cells and also towards the non-cancerous cell line MCF-10A, using the MTT reduction assay. From the 50% inhibitory concentration (IC_{50}) data listed in Table 6, it can be seen that the screened compounds reveal substantial action against cancerous cells, though much less than cisplatin. However, these ferrocenyl derivatives employ fewer toxic effects in normal cells. One plausible cause for the variance in action as related to that for cisplatin may lie in the difference in the approach of interaction with the DNA.[57] Cisplatin interacts covalently with nitrogenous bases in the DNA, while the synthesized complexes are assumed to experience electrostatic interactions as designated by electrochemical and spectroscopic studies. It is obvious from the Figure 8 that the tested compounds inhibited the growth of tumor cells in a dose-dependent fashion.

View Article Online
DOI: 10.1039/C8NJ00483H

Table 6. Cytotoxicity against human tumor and normal cells, after 72 h of incubation.

	IC_{50} (μM)	
Sample Code	**MCF-7**	**MCF-10A**
Cisplatin	1.55 ± 1.82	17.3 ± 0.59
M1	2.56 ± 1.01	16.6 ± 1.27
M2	3.24 ± 0.64	15.9 ± 0.74
M3	1.87 ± 1.07	17.0 ± 1.62
M4	4.02 ± 0.96	16.2 ± 0.95
M5	4.45 ± 1.25	15.7 ± 1.33
M6	4.99 ± 0.76	14.9 ± 0.88
M7	5.20 ± 1.19	13.8 ± 0.64
M8	5.91 ± 0.55	12.7 ± 0.97
M9	5.73 ± 1.47	13.3 ± 1.54

The results of the cytotoxicity assays indicate that those complexes bearing fluoro moiety on the phenyl ring show enhanced cell growth inhibitory effects as compared to the chloro and bromo containing molecules. This indicates that the presence of an electron-withdrawing group increases the polarity of these compounds, which in turn augments their lipophilicity and helps the molecules to interact or penetrate more through the cell membrane, thereby enhancing their cytotoxic action However, no particular cytotoxicity trend was observed by changing the position of the substituents from *ortho* to *para* on the benzoyl group.

View Article Online
DOI: 10.1039/C8NJ00483H

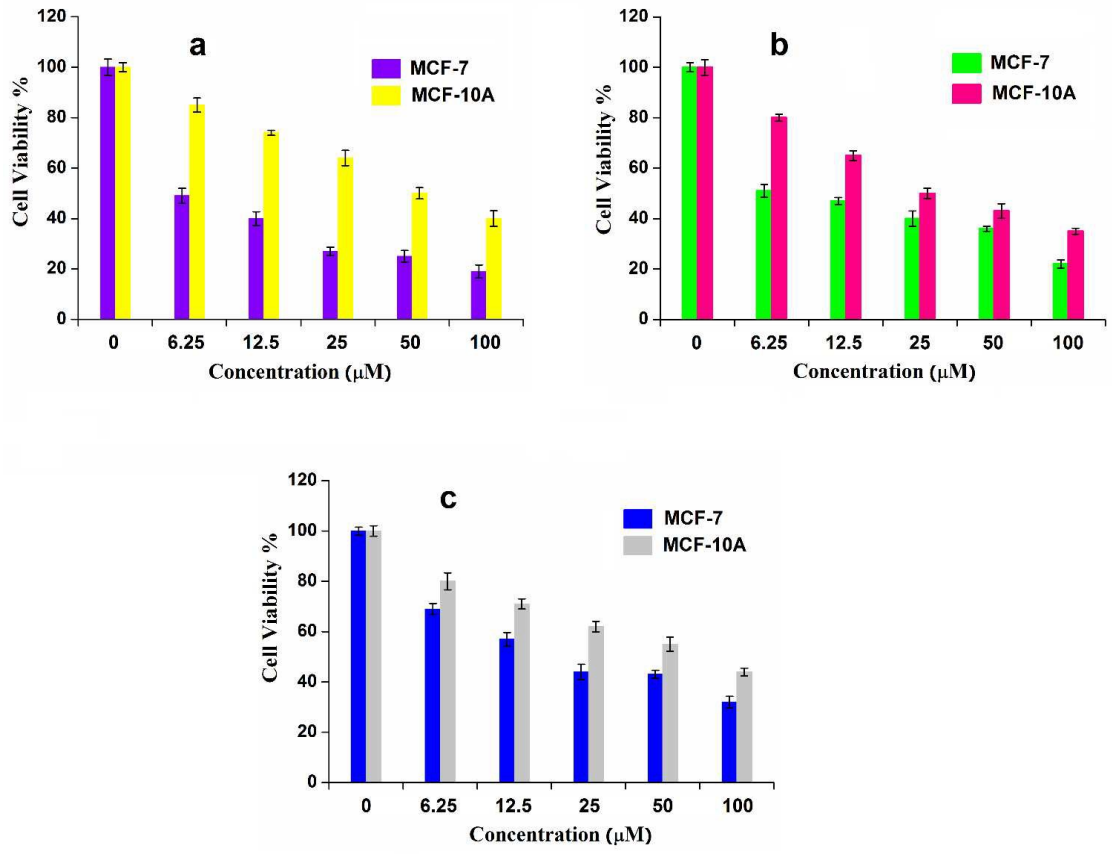

Figure 8. Cell viability (%) of cancerous and non-cancerous cells at various concentrations of (a) **M3**, (b) **M5**, and (c) **M7**, after 72 h of incubation.

The results of anticancer activity were found to be in close agreement with the DFT calculations. The anticancer activity of ferrocene derivatives is found to be dependent on the oxidation state of iron in the ferrocene moiety with some results indicating that the reduced Fe(II) ferrocenyl compound is more active than oxidized Fe(III) ones.[58] In the present study, a more negative E_{LUMO} and a small HOMO-LUMO band gap of **M3** favors the addition of electrons as the energies of the orbitals are reduced. Whereas, the complex **M8** has the least negative E_{HOMO} value and a large HOMO-LUMO band gap, which represents its ease of oxidation as compared to the other compounds.[27,45] Thus, **M3** complex with most negative E_{LUMO} and a small band gap favors the reduced form Fe(II) (more bioactive) in the ferrocene moiety, thus **M3** shows the highest growth inhibitory effect against the tumor cells.

4. Conclusions

Ferrocene-modified thioureas were synthesized and structurally characterized by various spectroscopic techniques, which validated the purity of these compounds. Moreover,

View Article Online
DOI: 10.1039/C8NJ00483H

DNA binding potentiality of the synthesized complexes was explored as a probable mechanism for the anticancer activity using DNA association constants evaluated by electrochemical and spectroscopic methods. These compounds have also been demonstrated to be promising candidates for inhibiting the microbial and tumor growth. The computational calculations based on DFT/B3LYP study correlate well with the cytotoxicity results. Thus, the insertion of a ferrocenyl moiety into thioureas has proved to be a significant approach to enhancing their therapeutic properties by augmenting their lipophilic character.

Conflicts of interest

There are no conflicts of interest to declare.

Acknowledgements

Faiza Asghar is highly obliged to the Higher Education Commission (HEC) of Pakistan for providing a scholarship under the program 5000 Indigenous PhD Scholarships at Quaid-i-Azam University, Islamabad and for a 6-month scholarship under the International Research Support Initiative Program (IRSIP) as a Graduate Research Trainee in the Department of Chemistry, McGill University, Montreal, Quebec, Canada.

References

[1] B. Rosenberg, L. Vancamp and T. Krigas, *Nature*, 1965, **205**, 698.

[2] B. Rosenberg, L. Vancamp, J. E. Trosko and V. H. Mansour, *Nature*, 1969, **222**, 385.

[3] T. Gianferrara, I. Bratsos and E. Alessio, *Dalton Trans*., 2009, **37**, 7588.

[4] C. G. Hartinger and P. J. Dyson, *Chem. Soc. Rev.*, 2009, **38**, 391.

[5] N. J. Long, *Metallocenes: An Introduction to Sandwich Complexes*, Blackwell Science, **1998**.

[6] A. Vessieres, S. Top, P. Pigeon, E. Hillard, L. Boubeker, D. Spera and G. Jaouen. *J. Med. Chem*., 2005, **48**, 3937.

[7] E. Hillard, A. Vessieres, F. Le Bideau, D. Plazuk, D. Spera, M. Huch and G. Jaouen. *ChemMedChem*., 2006, **1**, 551.

[8] S. Top, A. Vessieres, C. Cabestaing, I. Laios, G. Leclercq, C. Provot and G. Jaouen. *J. Organomet. Chem.*, 2001, **637**, 500.

[9] E. Hillard, A. Vessieres, L. Thouin, G. Jaouen and C. Amatore. *Angew. Chem. Int. Ed*., 2006, **45**, 285.

View Article Online
DOI: 10.1039/C8NJ00483H

[10] D. Osella, H. Mahboobi, D. Colangelo, G. Cavigiolio, A. Vessieres and G. Jaouen. *Inorg*. *Chim*. *Acta*., 2005, **358**, 1993.

[11] D. Osella, M. Ferrali, P. Zanello, F. Laschi, M. Fontani, C. Nervi and G. Cavigiolio. *Inorg. Chim. Acta*., 2000, **306**, 42.

[12] T. K. Venkatachalam, C. Mao and F. M. Uckun, *Bioorg. Med. Chem*., 2004, **12**, 4275.

[13] H. Zhang, L. Vrang, K. Backbro, P. Line, C. Sahlberg, T. Unge and B. O. Berg, *Antivir. Res*., 1995, **28**, 331.

[14] B. Lal, A. Badshah, A. A. Altaf, N. Khan and S. Ullah, *Appl. Organomet. Chem.*, 2011, **25**, 843.

[15] A. Saeed, R. A. Khera, N. Abbas, M. Latif, I. Sajid and U. Florke, *Turk. J. Chem*., **2010**, **34**, 335.

[16] M. Eweis, S. Elkholy and M. Elsabee, *Int. J. Biol. Macromol*., 2006, **38**, 1.

[17] D. Sriram, P. Yogeeswari, M. Dinakaran and R. Thirumurugan, *J. Antimicrob. Chemother*., 2007, **59**, 1194.

[18] S. Y. Ke and S. J. Xue, *Arkivoc.*, 2006, **10**, 63.

[19] M. S. Brouwer and A. C. Grosscurt, *Google Patents*, 1982.

[20] R. A. Hussain, A. Badshah and A. Shah, *Appl. Organomet. Chem*., 2014, **28**, 61.

[21] D. Gopi, N. Bhuvaneswaran, S. Rajeswarai and K. Ramadas, *Anti-Corrosion Methods Mater*., 2000, **47**, 332.

[22] J. S. Upadlgaya and P. K. Srivastava, *J. Ind. Chem. Soc*., 1982, **59**, 767.

[23] V. Alagarsamy, S. Meena, K. V. Ramseshu, V. R. Solomon, K. Thirumurugan, K. Dhanabal and M. Muruga, *Eur. J. Med. Chem*., 2006, **41**, 1293.

[24] F. Cui, Y. Cui, H. Luo, X. Yao, J. Fan and Y. Lu, *Chin. Sci. Bull.*, 2006, **51**, 2201.

[25] F. Asghar, S. Fatima, S. Rana, A. Badshah, I. S. Butler and M. N. Tahir, *Dalton Trans*., 2018, **47**, 1868.

[26] F. Asghar, A. Badshah, I. S. Butler, S. Tabassum, B. Lal and M. N. Tahir, *Inorg. Chim. Acta*., 2016, **442**, 46.

[27] F. Asghar, A. Badshah, S. Fatima, S. Zubair, I. S. Butler and M. N. Tahir, *J. Organomet. Chem*., 2017, **843**, 48.

[28] B. Lal, A. Badshah, A. A. Altaf, M. N. Tahir, S. Ullah and F. Huq, *Dalton Trans*., 2012, **41**, 14643.

[29] F. Asghar, A. Badshah, A. Shah, M. K. Rauf, M. I. Ali, M. N. Tahir, E. Nosheen, R. Zia ur and R. Qureshi, *J. Organomet. Chem*., 2012, **717**, 1.

[30] R. L. Scott, *Recl. Trav. Chim. Pays-Bas*., 1956, **75**, 787.

View Article Online
DOI: 10.1039/C8NJ00483H

[31] M. Sirajuddin, S. Ali, N. A. Shah, M. R. Khan and M. N. Tahir, *Spectrochim. Acta A*., 2012, **94**, 134.

[32] S. J. Smith and B. T. Sutcliffe, *Rev. Comput. Chem*., 1997, **70**, 271.

[33] Atta-ur-Rahman, M. I. Choudhary and W. J. Thomesen, *Bioassay Techniques for Drug Development*, Harwood Academic Publishers, Amsterdam., 2001, 9.

[34] D. Kalemba and A. Kunicka, *Curr. Med. Chem*., 2003, **10**, 813.

[35] B. Lal, A. Badshah, A. A. Altaf, M. N. Tahir, S. Ullah and F. Huq, *Aus. J. Chem*., 2013, **41**, 14643.

[36] T. Mosmann, *J. Immunol. Methods*., 1983, **65**, 55.

[37] Q. Feng, N. Q. Li and Y. Y. Jiang, *Anal. Chim. Acta*., 1997, **344**, 97.

[38] M. Aslanoglu and G. Ayne, *Anal. Bioanal. Chem*., 2004, **380**, 658.

[39] A. M. Oliveira-Brett, J. Piedade, L. Silva and V. Diculescu, *Anal. Biochem*., 2004, **332**, 321.

[40] A. M. Oliveira-Brett, V. Diculescu and J. A. P. Piedade, *Bioelectrochemistry*., 2002, **55**, 61.

[41] A. Shah, R. Qureshi, N. K. Janjua, S. Haque and S. Ahmed, *Anal. Sci*., 2008, **24**, 1437.

[42] F. Asghar, A. Badshah, B. Lal, I. S. Butler, S. Tabassuma and M. N. Tahir, *Inorg. Chim. Acta.,* 2016, **439**, 82.

[43] M. K. Rauf, U. Shaheen, F. Asghar, A. Badshah, A. Nadhman, S. Azam, M. I. Ali, G. Shahnaz and M. Yasinzai, *Arch. Pharm. Chem. Life Sci*., 2015, **349**, 50.

[44] M. Aslanoglu, *Anal. Sci*., 2006, **22**, 439.

[45] F. Asghar, A. Badshah, B. Lal, S. Zubair, S. Fatima and I. S. Butler, *Bioorg. Chem*., 2017, **72**, 215.

[46] R. Gul, A. Badshah, A. Khan, A. Junaid and M. K. Rauf, *Spectrochim. Acta A*., 2014, **117**, 264.

[47] R. Fukuda, S. Takenaka and M. Takagi, J. *Chem. Soc. Chem. Commun*., **1990**, 1028.

[48] C. Cantor and P. R. Schimmel, *Biophysical Chemistry*, W. H. Freeman, San Francisco, **1980**.

[49] C. C. Ju, A. G. Zhang, C. L. Yuan, X. L. Zhao and K. Z. Wang, *J. Inorg. Biochem*., 2011, **105**, 435.

[50] F. Asghar, A. Badshah, R. A. Hussain, M. Sohail, K. Akbar and I. S. Butler, *J. Organomet. Chem*., 2015, **797**, 131.

[51] C. Lee, W. Yang, R. G. Parr, *Phys. Rev. B*., 1998, **37**, 785.

View Article Online
DOI: 10.1039/C8NJ00483H

[52] Y. Ataly, D. Avci, A. BaSoglu, *J. Struct. Chem.*, 2008, **19**, 239.

[53] S. Fatima, A. Badshah, B. Lal, F. Asghar and M. N. Tahir, *J. Organomet. Chem*., 2016, **819**, 194.

[54] M. Marinov, S. Minchev, N. Stoyanov, G. Ivanova and M. Spassova, *Croat. Chem. Acta*., 2005, **78**, 9.

[55] B. W. D. Andrade, S. Datta, S. R. Forrest, P. Djurovich, E. Polikarpov and M. E. Thompson, *Org. Electron*., 2005, **6**, 11.

[56] S. Chandrasekar, V. Balachandran, H. S. Evans, and A. Latha, *Spectrochim. Acta A*., 2015, **143**, 136.

[57] H. Tayyem, F. Huq, J. Q. Yu, P. Beale and K. Fisher, *Chem Med Chem*., 2008, **3**, 145.

[58] M. F. R. Fouda, M. M. Abd-Elzaher, R. A. Abdelsamaia and A. A. Labib, *Appl. Organomet. Chem*., 2007, **21**, 613.

View Article Online
DOI: 10.1039/C8NJ00483H

The DNA binding affinity of ferrocenyl complexes explored by CV and UV ascertain them as noble DNA binders. The computational measurements correlate well with the outcomes of electrochemistry and bio-activities.

View Article Online
DOI: 10.1039/C8NJ00483H

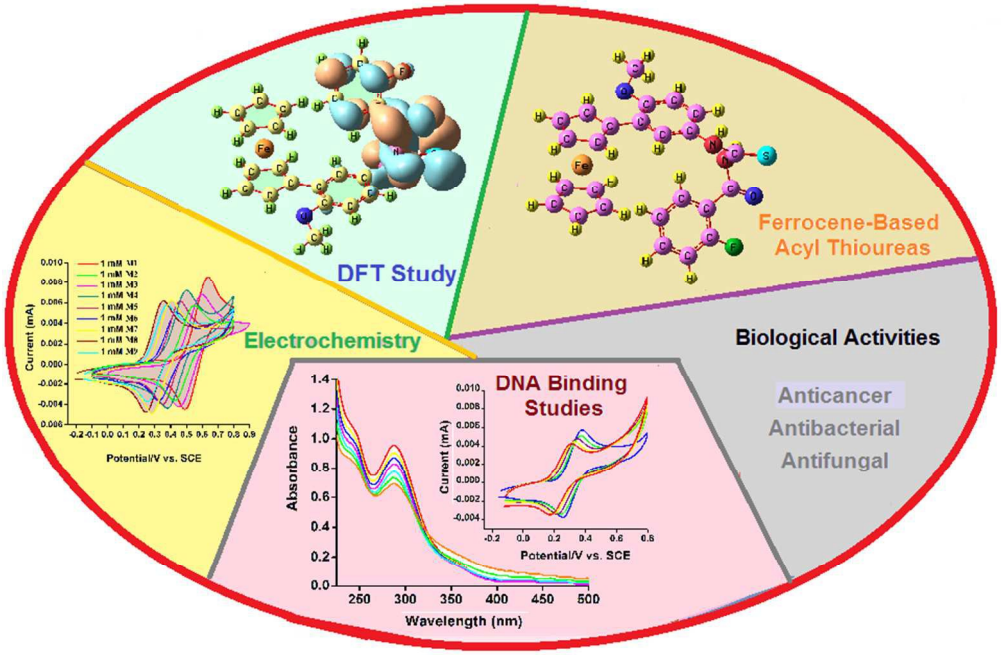

254x167mm (96 x 96 DPI)